NANO LETTERS

Supplementary Information

Assembly of Polygonal Nanoparticle Clusters Directed by Reversible Noncovalent Bonding Interactions

REVISED VERSION

Mark A. Olson, Ali Coskun, Rafal Klajn, Lei Fang, Sanjeev K. Dey, Kevin Browne, Bartosz A. Grzybowski*, and J. Fraser Stoddart*

Department of Chemistry and Department of Chemical and Biological Engineering, Northwestern University, Evanston, Illinois 60208

* To Whom Correspondence should be Addressed	
Professor J Fraser Stoddart Department of Chemistry Northwestern University 2145 Sheridan Road Evanston, Illinois 60208-3113 Tel: (+1)-847-491-3793 Fax: (+1)-847-491-1009 E-Mail: stoddart@northwestern.edu	**Professor Bartosz A. Grzybowski** Department of Chemical and Biological Engineering Northwestern University 2145 Sheridan Road Evanston, Illinois 60208-3113 Tel: (+1)-847-491-3113 Fax: (+1)-847-491-3728 E-Mail: grzybor@northwestern.edu

General Methods: All solvents (Fischer Science) were dried prior to use. All reagents and starting materials were purchased from Aldrich or VWR and used without further purification. **4**,[S1] **5**,[S1] **6**·4PF_6,[S2] **7**,[S3] **8**,[S4] **9**,[S5] **11**·2PF_6,[S6] and **13**[S7] were prepared according to published literature procedures. Thin-layer chromatography was carried out using aluminum sheets precoated with silica gel 60 (Merck 40 – 60 mm, 230 – 400 mesh). High Performance Liquid Chromatography (HPLC) purification was performed on a preperative reversed phase-HPLC (RP-HPLC) instrument, using a C18 column. Column chromatography was performed on silica gel 60 (Merck 40–60 nm, 230–400 mesh). Deuterated solvents (Cambridge Isotope Laboratories) for NMR spectroscopic analyses were used as received. NMR Spectra were recorded on Varian INOVA-500 (at 500 MHz) as well as on Bruker 500 and 600 MHz spectrometers. All chemical shifts are quoted in ppm, relative to tetramethylsilane, using the residual solvent peak as a reference standard. Mass spectra were measured on an IonSpec 7.0T Ultima FTMS with ESI and matrix-ssisted laser desorption/ionization (MALDI) ion sources.

Scheme S1. Synthesis of 1·8PF_6

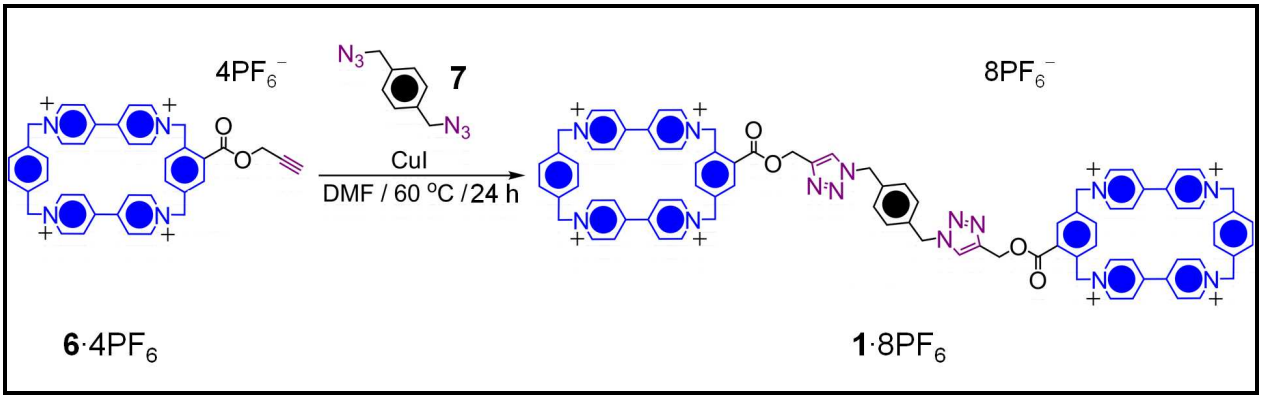

1·8PF_6: A mixture of the α,α'-diazido-*p*-xylene **7** (5 mg, 0.027 mmol) and the $CBPQT^{4+}$ alkyne derivative **6**·4PF_6 (63 mg, 0.053mmol) was added to DMF-d_7 (1 mL) in a dry NMR tube and was degassed by bubbling Ar through the solution for 2 h. An ^{1}H NMR spectrum of this mixture was

recorded at this juncture. CuI (15 mg, 0.079 mmol) was then added to the reaction mixture. The reaction, which was heated to 60°C in a sand-bath for 24 h, was monitored by ^{1}H NMR spectroscopy. The reaction mixture was cooled and washed with aqueous EDTA. The organic material was dissolved by MeCN (2 mL) and then added dropwise to a saturated aqueous NH_4PF_6 solution (50 mL) to precipitate the product. The precipitate was recovered by filtration to afford the **1**·8PF_6 as a crystalline white solid (41 mg, 60 %); ^{1}H NMR (DMF-d_7, 500 MHz, 25°C): δ = 5.61 (s, 4H), 5.81 (s, 4H), 6.18 (s, 8H), 6.25 (s, 4H), 6.49 (s, 4H), 7.50 (s, 4H), 7.99 (s, 7H), 8.02 (s, 1H), 8.04 (d, *J* = 5 Hz, 4H), 8.10 (d, *J* = 5 Hz, 2H), 8.52 (s, 2H), 8.59 (s, 2H), 8.69 (d, *J* = 5 Hz, 4H), 8.81 (m, 12H), 9.60 (d, *J* = 5 Hz, 4H), 9.70 (d, *J* = 5 Hz, 4H), 9.75–9.78 (m, 8H); ^{13}C NMR (DMF-d_7, 125 MHz, 25°C): δ = 53.1, 53.8, 59.4, 61.2, 63.7, 64.4, 64.5, 125.7, 126.9, 127.1, 127.2, 127.4, 128.7, 128.9, 129.1, 130.5, 130.7, 130.8, 132.6, 133.6, 134.5, 136.6, 136.8, 137.3, 137.4, 137.6, 146.0, 146.3, 146.6, 148.20, 148.24, 148.5, 148.6, 166.5; ESI-HRMS: *m/z* calcd for 2552.33; found: 1131.2004 $[M - 2PF_6]^{2+}$.

Scheme S2. Synthesis of 2·12PF_6

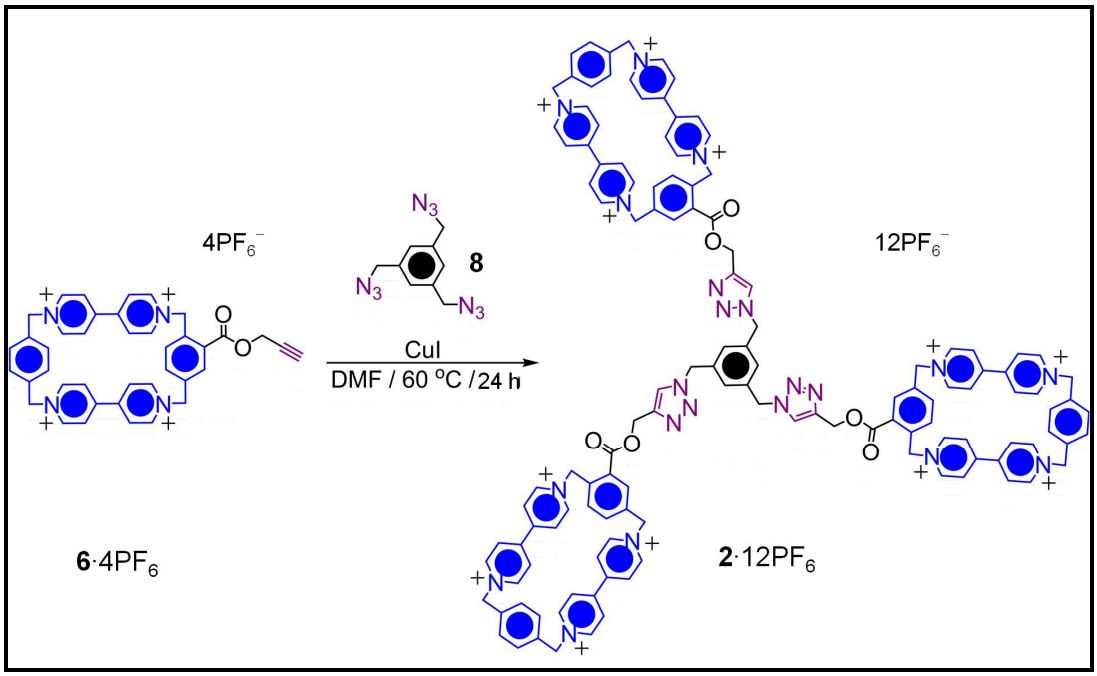

2·12PF$_6$: A mixture of the triazide **8** (7.6 mg, 0.031 mmol) and the CBPQT^{4+} alkyne derivative **6**·4PF$_6$ (111 mg, 0.094 mmol) was added to DMF-d_7 (1 mL) in a dry NMR tube and it was degassed by bubbling Ar through the solution for 2 h. An ^{1}H NMR spectrum of this mixture was recorded at this juncture. CuI (15 mg, 0.079 mmol) was then added to the reaction mixture. The reaction, which was heated to 60°C in a sand-bath for 24 h, was followed by ^{1}H NMR spectroscopy. The reaction mixture was cooled and washed with aqueous EDTA. The organic material was dissolved by MeCN (2 mL) and then added dropwise to a saturated aqueous NH_4PF_6 solution (50 mL) to precipitate the product. The precipitate was recovered by filtration to afford the **2**·12PF$_6$ as a crystalline white solid (98 mg, 82 %); ^{1}H NMR (DMF-d_7, 500 MHz, 25°C): δ = 5.46 (s, 6H), 5.61 (s, 6H), 5.76 (d, J = 5 Hz, 12H), 5.83 (s, 6H), 6.15 (s, 6H), 7.29 (s, 3H), 7.53–7.56 (m, 14H), 7.64 (d, J = 5 Hz, 3H), 8.05 (s, 3H), 8.09 (d, J = 5 Hz, 4H), 8.19–8.20 (m, 20H), 8.88 (d, J = 10 Hz, 12H), 8.91 (d, J = 10 Hz, 12H); ^{13}C NMR (CD_3CN, 125 MHz, 25°C): δ = 53.8, 59.9, 62.4, 64.9, 65.60, 65.63, 83.9, 126.1, 127.8, 128.2, 128.3, 128.4, 128.5, 131.1, 131.2, 131.3, 133.4, 134.4, 134.9, 136.8, 136.9, 137.0, 137.3, 138.3, 143.1, 146.1, 146.2, 146.8, 150.4, 150.5, 150.8, 168.8; ESI-HRMS: *m/z* calcd for 3789.47; found: 1749.73 [M – 2PF$_6$]$^{2+}$; 1118.15 [M – 3PF$_6$]$^{3+}$; 802.36 [M – 4PF$_6$]$^{4+}$

Scheme S3. Synthesis of 12·4PF$_6$

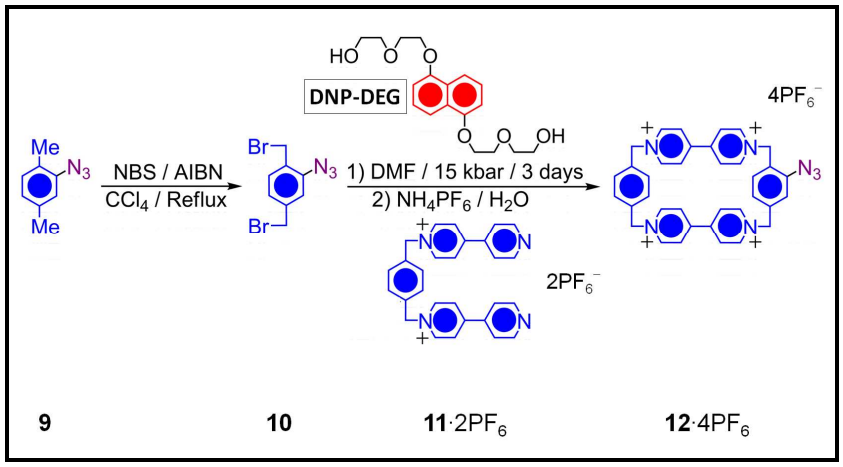

10: **9** (280 mg, 1.9 mmol), NBS (747 mg, 4.2 mmol), and AIBN (60 mg, 0.37 mmol) in dry CCl_4 (50 mL) were heated under reflux for 12 h. The mixture was cooled and filtered to remove insoluble solid. The solvent was then evaporated under reduced pressure and purified by silica gel column chromatography [SiO_2: CH_2Cl_2 / Hexane, (1 : 6)] to give **10** as a white solid (348 mg, 60%). ^{1}H NMR (500 MHz, $CDCl_3$, 298 K): δ = 4.46 (s, 2H), 4.47 (s, 2H), 7.14 (dd, *J* = 7.8 Hz, *J* = 1.4 Hz, 1H), 7.18 (d, *J* = 1.4 Hz, 1H), 7.35 (d, *J* = 7.8 Hz, 1H) ppm. ^{13}C NMR (125 MHz, $CDCl_3$, 298 K): δ = 26.7, 30.9, 117.9, 124.6, 127.9, 130.7, 138.0, 138.9 ppm. EI-HRMS *m/z* calcd for 302.9007; found 302.9001 $[M]^+$.

12·4PF$_6$: **11**·2PF_6 (517 mg, 0.73 mmol) was added to a solution of **10** (223 mg, 0.73 mmol) and the template **DNP-DEG** (738 mg, 2.2 mmol) dissolved in DMF (10 mL). The reaction mixture was subjected to high pressure (10 – 15 kbar) for 3 days. The solvent was removed from the resulting purple solution under vacuum, and the purple oil was subjected to liquid-liquid extraction [$CHCl_3$ / 1 % (w / v) NH_4Cl (aq)] until the solution became colorless (5 days). The solvent was removed from the aqueous portion and the resulting solid was subjected to column chromatography [SiO_2: MeOH / $MeNO_2$ / 2 M NH_4Cl (7 : 1 : 2)]. The eluent was removed in vacuo, the solid was dissolved in hot H_2O and a saturated aqueous solution of NH_4PF_6 was added until no further precipitate was observed. The precipitate was recovered by filtration to give the appropriate tetracationic cyclophane as its tetrakis(hexafluorophosphate) salt. The compound was further purified by RP-HPLC (H_2O – MeCN / 0 – 100 % in 40 min, λ = 254 nm) to give **12**·4PF_6 (350 mg, 42 %). ^{1}H NMR (500 MHz, CD_3CN, 298 K): δ = 5.71 (s, 2H), 5.76 (s, 2H), 5.79 (s, 2H), 7.36 (d, *J* = 1.4 Hz, 1H), 7.47 (dd, *J* = 7.8 Hz, *J* = 1.4 Hz, 1H), 7.58 (s, 4H), 7.69 (d, *J* = 7.8 Hz, 1H), 8.16 (d, *J* = 6.8 Hz, 2H), 8.21 - 8.24 (m, 6H), 8.92 – 8.96 (m, 8H) ppm. ^{13}C NMR (125 MHz, CD_3CN, 298 K): δ = 60.0, 63.8, 64.3, 119.8, 125.8, 125.9, 126.4, 126.97,

126.98, 127.1, 129.8, 129.9, 132.4, 135.6, 135.7, 137.4, 140.3, 144.8, 144.90, 144.95, 145.5, 148.9, 149.0, 149.1, 149.2 ppm. ESI-HRMS *m/z* calcd for 996.1561; found: 996.1571 $[M - PF_6]^+$; 425.5962 $[M - 2PF_6]^{2+}$.

Scheme S4. Synthesis of 3·16PF$_6$

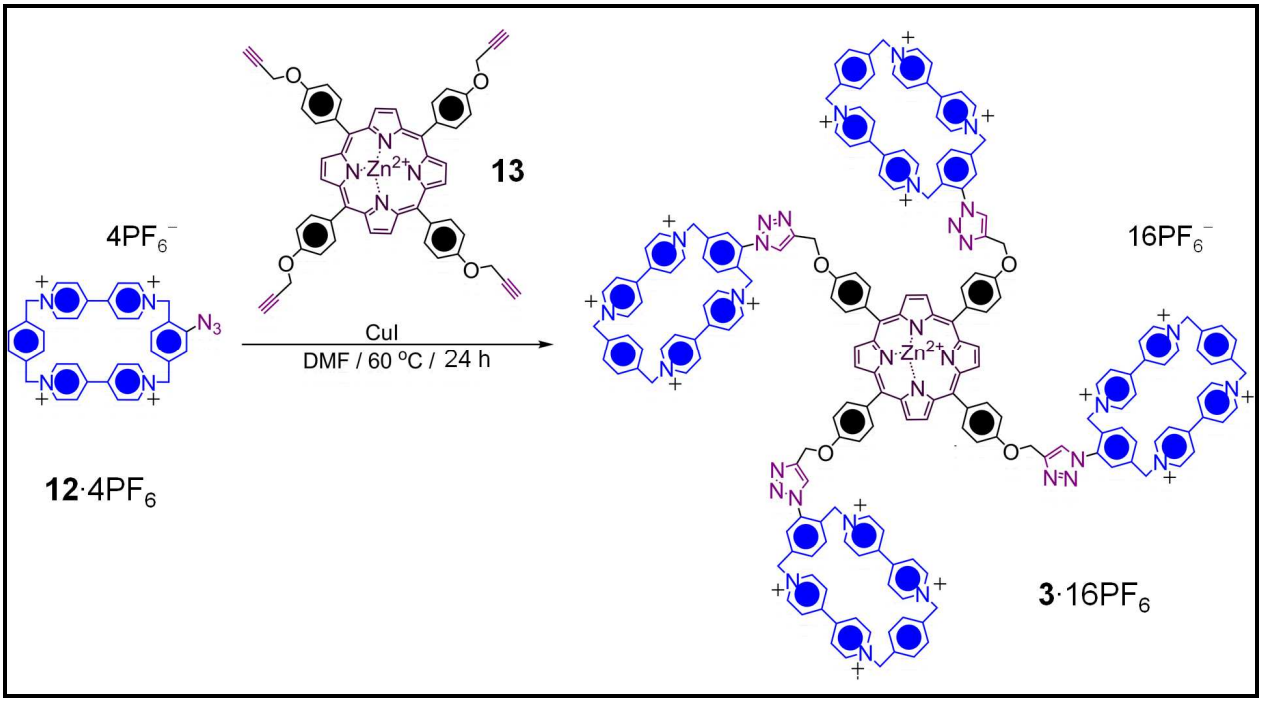

3·16PF$_6$: A mixture of **12**·4PF$_6$ (120 mg, 0.105 mmol) and tetra-alkynyl porphyrin derivative **13** (22.4 mg, 0.025 mmol) was dissolved in dry DMF (4 mL) and the mixture was degassed by bubbling Ar through the solution for 30 min. CuI (24 mg, 0.125 mmol) was then added to the reaction mixture. The reaction mixture was heated to 60°C for 24 h. After the reaction was completed, the reaction mixture was cooled and washed with aqueous EDTA solution. Crude product was further purified by RP-HPLC (H_2O – MeCN / 0 – 100 % in 40 min, λ = 254 nm). The violet-colored fraction was collected and solvent removed under reduced pressure. The resulting solid was dissolved in a minimal amount of Me_2CO and the solution was added dropwise to a saturated aqueous NH_4PF_6 solution (10 mL) to precipitate out the product. The

precipitate was recovered by filtration to afford **3**·16PF_6 as a purple solid (55 mg, 40 %); ^{1}H NMR (500 MHz, CD_3CN, 298 K): δ = 5.53 (s, 8H), 5.91 (s, 8H), 5.99 (s, 8H), 6.18 (s, 8H), 6.24 (s, 8H), 7.48 (d, *J* = 8.5 Hz, 8H), 7.56 (s, 16H), 7.52 – 7.70 (m, 12H), 8.02 (s, 4H), 8.11 (d, *J* = 8.5 Hz, 8H), 8.34 – 8.38 (m, 12H), 8.46 – 8.52 (m, 20H), 8.85 (s, 8H), 8.88 (d, *J* = 6.9 Hz, 8H), 9.16 (d, *J* = 6.9 Hz, 8H), 9.21 (d, *J* = 6.9 Hz, 8H), 9.31 (s, 8H) ppm. ^{13}C NMR (125 MHz, CD_3CN, 298 K): δ = 61.5, 62.2, 64.6, 65.4, 113.8, 121.1, 127.3, 127.8, 128.1, 128.3, 128.5, 131.1, 131.2, 131.3, 131.5, 132.3, 132.4, 134.4, 136.4, 136.5, 136.8, 136.9, 137.0, 137.4, 138.7, 138.8, 140.6, 144.4, 144.5, 145.7, 145.8, 146.2, 146.4, 146.5, 146.6, 150.4, 150.5, 150.7, 151.0, 151.1, 151.2, 157.0, 159.1 ppm. ESI-HRMS *m/z* calcd for 1673.9306; found: 1673.8983 $[M - 3PF_6]^{3+}$; 1219.2163 $[M - 4PF_6]^{4+}$.

Scheme S5. Preparation of 4/5-AuNPs

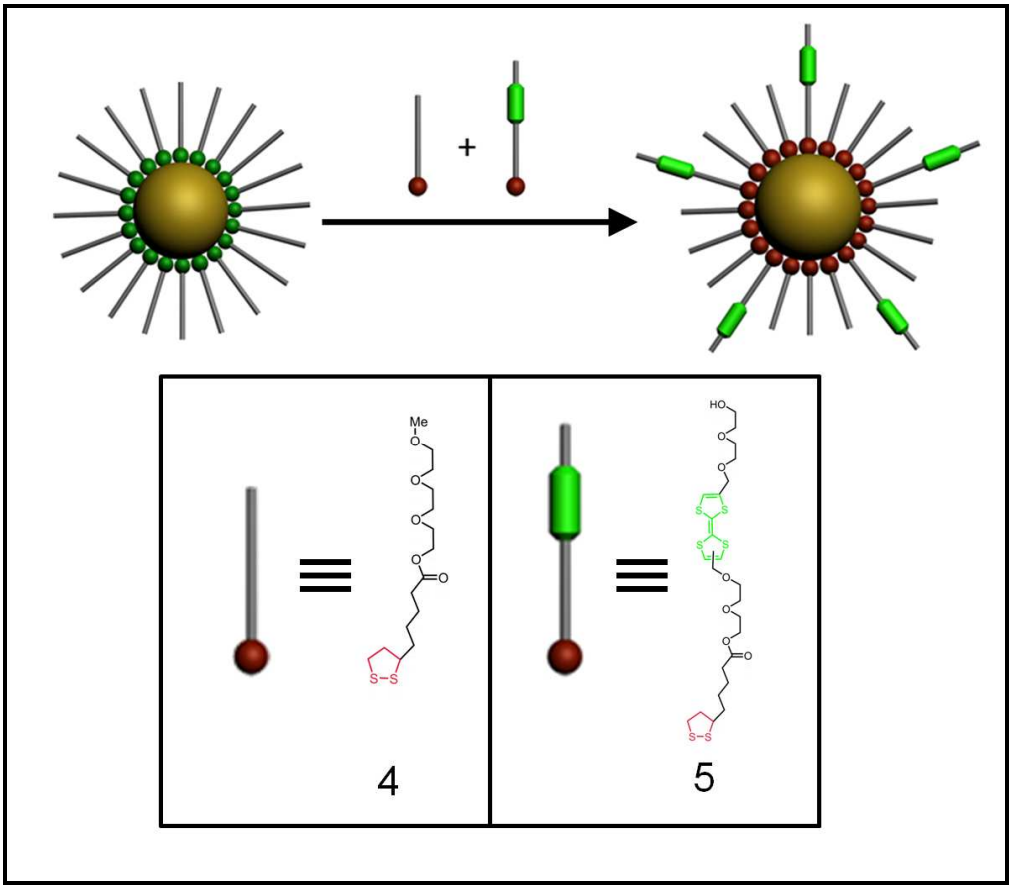

Preparation of "Precursor" Gold Nanoparticles

The synthesis was based on a modified literature procedure[S7]. A solution of $HAuCl_4 \cdot 3H_2O$ (0.300 mmol; 118 mg) H_2O (10 mL) was added to a solution of tetraoctylammonium bromide (TOAB; 1.40 mmol; 766 mg) in PhMe (28 mL). Under vigorous stirring, the transfer of gold to the organic phase was complete in 15 min. Gold was then reduced by a dropwise addition of a solution of $NaBH_4$ (3.20 mmol) in H_2O. The solution was stirred for 1 h to give $d = 4.58 \pm 1.23$ nm AuNPs in PhMe. AuNPs of this diameter are composed of ~2,960 atoms (based on the density of gold) and can harbor up to ~77 dithiolane ligands per NP (based on a surface area occupied by a single thiolane ligand, SA = 0.214 nm^2).[S8]

Functionalization of "Precursor" Nanoparticles

***General considerations*:** The AuNP solutions (500 μL; $5.35 \cdot 10^{-3}$ mmol in terms of gold atoms) were diluted twice with PhMe and added to a mixture of **4** and **5**; (total dithiolane concentration, c_{DT} = 2 mM; total dithiolane molarity; $n_{DT} = 5 \times 10^{-6}$ mol; this molarity corresponds to ca. 10-fold excess of ligands with respect to the number of binding sites on NPs) in PhMe. After 1 h, hexane (2 mL) was added to induce the precipitation of the nanoparticles. Black solids were collected by centrifugation, washed three times with PhMe to remove excess of ligands, dried with a nitrogen stream, and redissolved in pure MeCN.

χ = 0.050 AuNPs: These nanoparticles were prepared using a 1:20 molar ratio of **5** and **4**. They had an average of 11.5 TTF ligands per nanoparticle.

χ_{TTF} = 0.0065 AuNPs ("Monofunctionalized"): Molar ratio of **5** and **4** used for the functionalization procedure corresponded 1 to 3,000 (typically, we used 1 μL and 3 mL of 10 mM PhMe solutions of **5** and **4**, respectively). This protocol allowed us to obtain

"monofunctionalized" (χ_{TTF} = 0.0065) nanoparticles in a ~1:13 mixture with non-functionalized nanoparticles (that is, covered entirely by **5**; χ_{TTF} = 0.0).

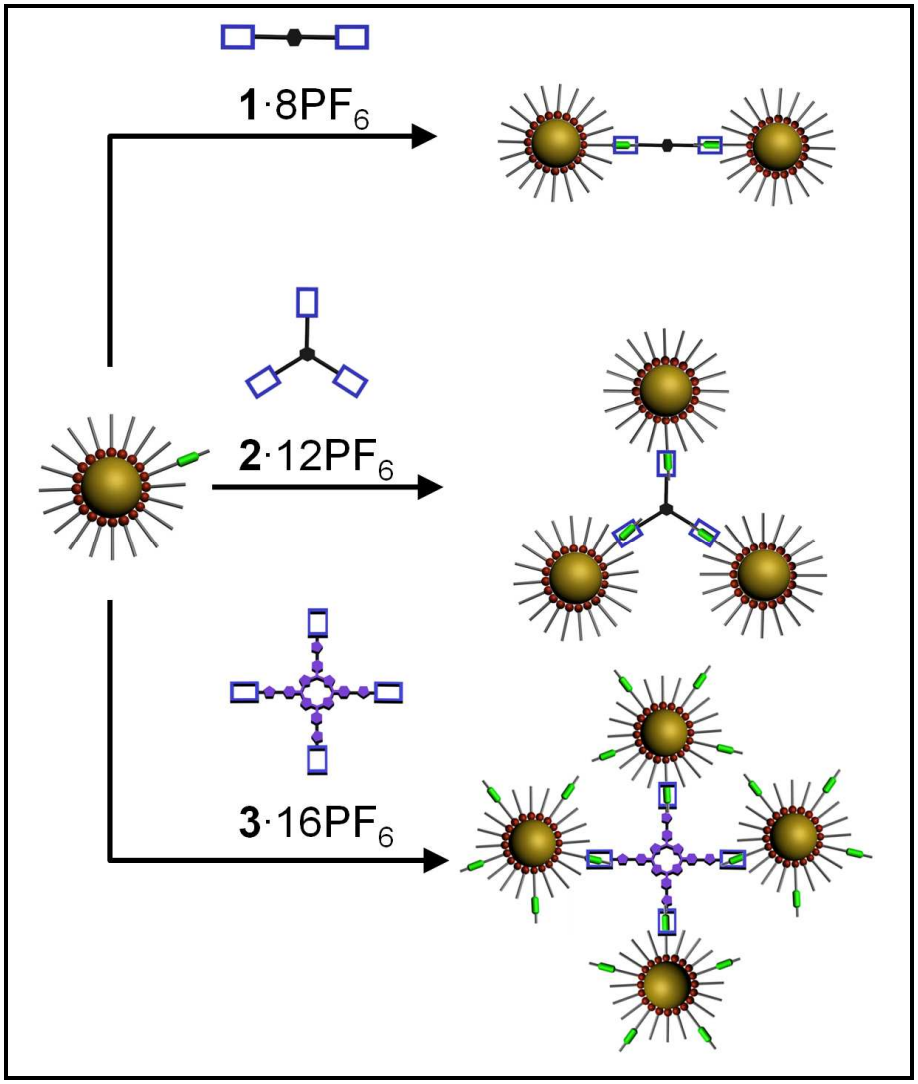

Selective Self-Assembly of 4/5-AuNPs into Dimers, Trimers and Tetramers

In a typical procedure, solutions of **4/5**-AuNPs in MeCN (χ = 0.050 or χ_{TTF} = 0.013 AuNPs) were diluted with MeCN to the final AuNP concentration, c_{NP} = 0.17 μM (in terms of Au NPs, this concentration corresponds to c_{Au} = 0.50 mM in terms of Au atoms). Varying amounts of **1**·8PF_6, **2**·12PF_6 and **3**·16PF_6 solutions in MeCN were then added and the samples were imaged on a JEOL 2100F transmission electron microscope.

Additional Spectroscopic Characterization

The azide-alkyne Huisgen 1,3 dipolar-cycloaddition reaction for the formation of **1**·8PF_6 was followed by ^{1}H NMR spectroscopy (Figure S1) at time zero (a) and after 3 h (b). The appearance of a singlet (δ = 8.55 ppm) for the triazole protons can be observed. Additionally, the chemical shift of the propargyl methylene protons (–$CO_2C\mathbf{H}_2C{\equiv}CH$, δ = 5.30 ppm) of the unreacted **6**·4PF_6 can be observed at δ = 5.8 ppm in **1**·8PF_6 for the –$CO_2C\mathbf{H}_2$–triazole protons. The methylene protons in the diazide unit (–$C\mathbf{H}_2N_3$, δ = 4.70 ppm) can also be observed to have undergone (–$OCH_2C\mathbf{H}_2$–triazole, δ = 5.60 ppm) sizable downfield shifts on triazole formation. The chemical shifts of the peaks for the protons in unreacted **6**·4PF_6, and of the diazide **7** protons indicate complete conversion after 3 h, with no further spectroscopic changes being evident after 24 h.

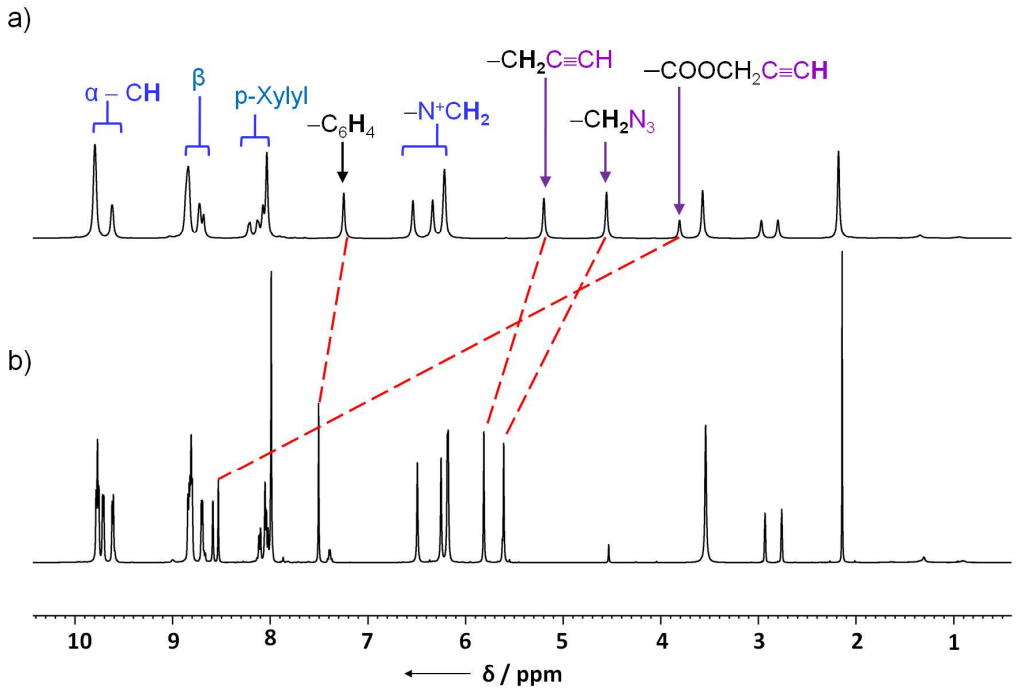

Figure S1. Stacked ^{1}H NMR spectra recorded in DMF-d_7 at 298 K following the click reaction for the formation of **1**·8PF_6 at (a) time = 0 and (b) time = 3 h.

The azide-alkyne cycloaddition reaction for the formation of **2**·12PF_6 was monitored by ^{1}H NMR spectroscopy (Figure S2) at time zero (a) and after 3 h (b). The appearance of a singlet (δ = 8.55 ppm) for the triazole protons can be observed. Additionally, the chemical shift of the propargyl methylene protons (–$CO_2C\mathbf{H}_2C{\equiv}CH$, δ = 5.30 ppm) of unreacted **6**·4PF_6 can be observed at δ = 5.95 ppm in **2**·12PF_6 for the –$CO_2C\mathbf{H}_2$–triazole protons. The methylene protons in the triazide unit (–$C\mathbf{H}_2N_3$, δ = 4.75 ppm) can also be observed to have undergone (–$OCH_2C\mathbf{H}_2$–triazole, δ = 5.75 ppm) sizable downfield shifts on triazole formation. The chemical shifts of the peaks for the protons in unreacted **6**·4PF_6, and of the triazide **8** protons indicate complete conversion after 3 h, with no further spectroscopic changes being evident after 24 h.

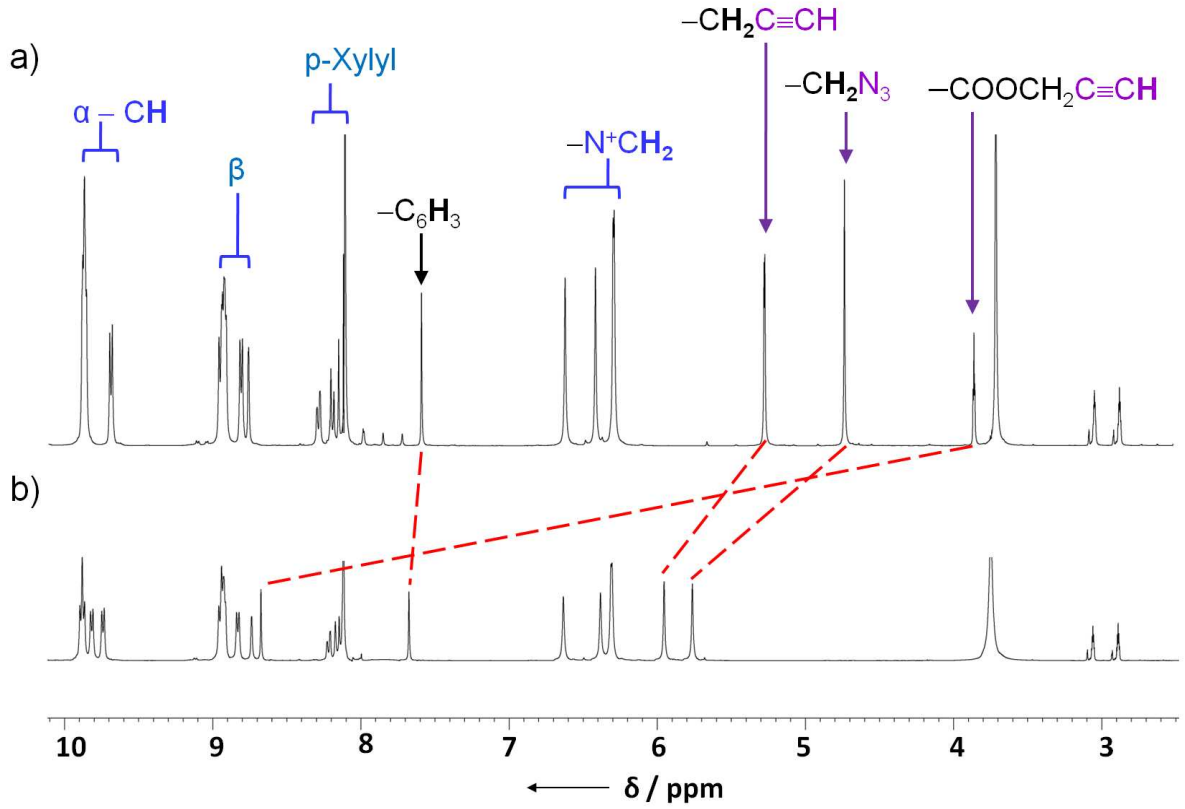

Figure S2. (a) Stacked ^{1}H NMR spectra recorded in DMF-d_7 at 298 K following the click reaction for the formation of **2**·12PF_6 at (a) time = 0 and (b) time = 3 h.

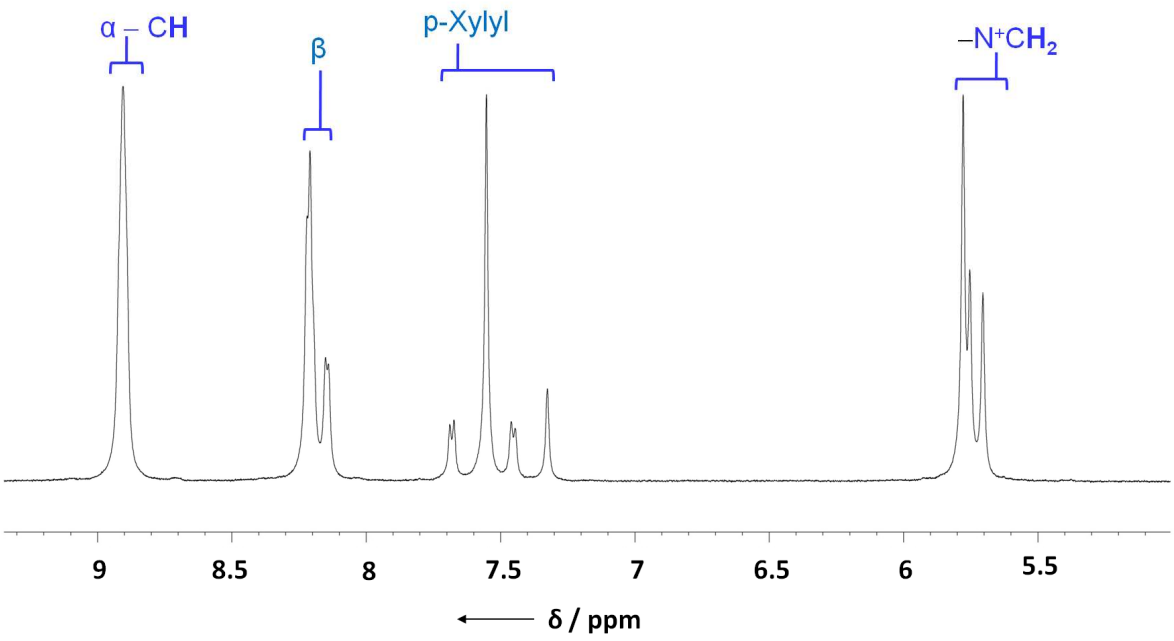

Figure S3. ^{1}H NMR spectra of the azide-functionalized CBPQT^{4+} derivative **12**·4PF$_6$ recorded in CD_3CN at 298 K.

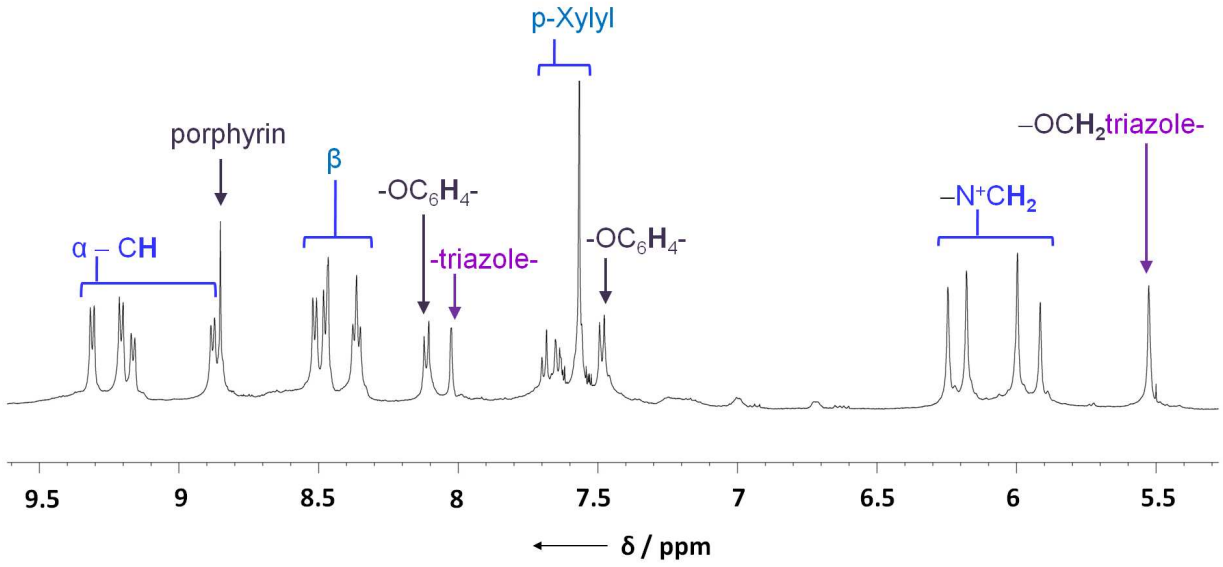

Figure S4. ^{1}H NMR spectra of tetra-CBPQT^{4+} derivative **3**·16PF$_6$ recorded in CD_3CN at 298 K

Optimized Potentials for Liquid Simulations (OPLS 2005) Minimized Geometries

To obtain approximate dimensions for the templates, optimized geometries for superstructures **1**·8PF_6 (Figure S5), **2**·12PF_6 (Figure S6), and **3**·16PF_6 (Figure S7) were calculated using OPLS 2005 force field[S9] energy minimization, with no solvent model, and a constant dielectric value of 1. The calculated distances have been rounded to the nearest hundredth of a nanometer.

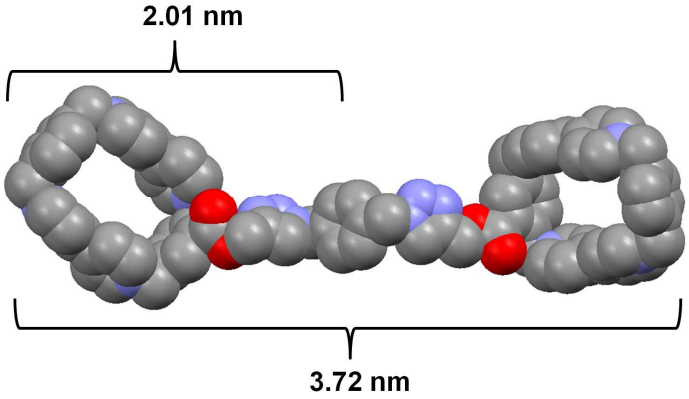

Figure S5. OPLS 2005-optimized geometry for the superstructure template **1**·8PF_6

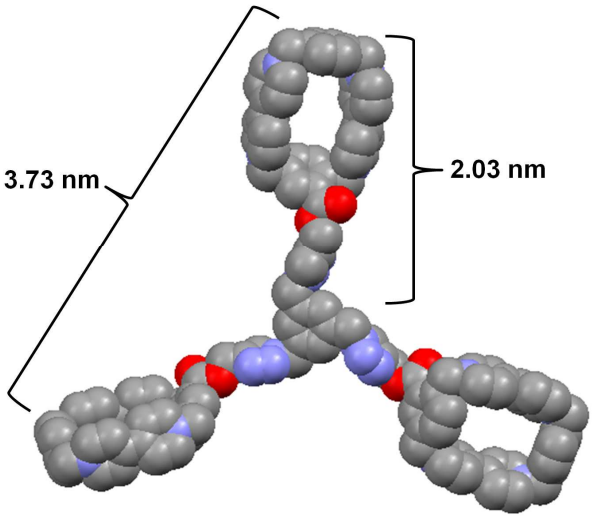

Figure S6. OPLS 2005-optimized geometry for the superstructure template **2**·12PF_6

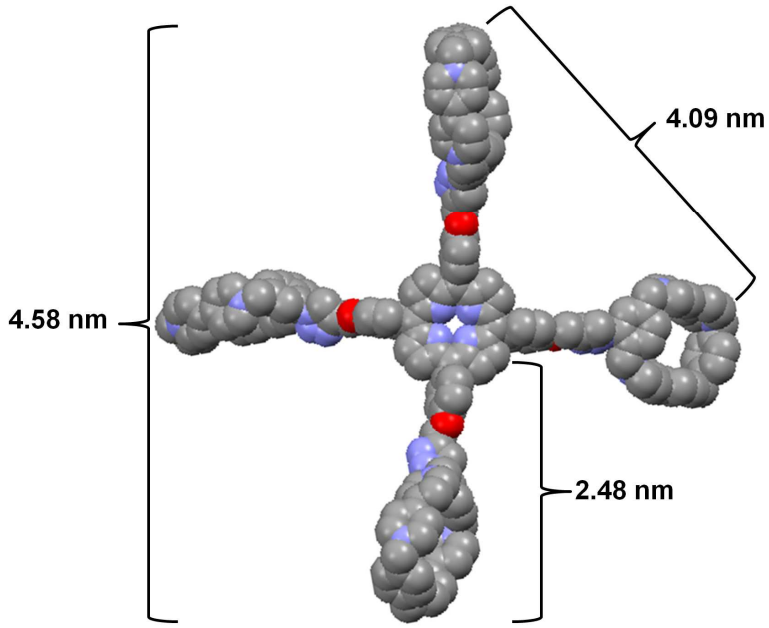

Figure S7. OPLS 2005-optimized geometry for the superstructure template **3**·16PF_6

Additional HR-TEM Images

Following the template-directed systemization of the AuNPs into discrete homo-dimers, trimers, and tetramers, HR-TEM was employed to image the nanoparticle assemblies and their atomic arrangements. We investigated the possibility of processing the reversible assemblies into permanent polygonal structures. Specifically, we have used the phenomenon of nanoparticle coalescence upon removal of the SAMs protecting the proximal NPs. Thermal treatment at temperatures above 95 ^{o}C causes desorption of the thiolates from the gold surface simultaneously fusing the nanoparticles, a process which is driven by the minimization of the overall surface tension.[S10] A focused electron beam was used to achieve elevated temperatures on the order of several hundred ^{o}C, sufficient enough to melt the templated assemblies rapidly into rod-like, triangular, and square-like nanostructures. The coalescence process can be observed when the assemblies were imaged over time. In the case of the coalescing trimers (Figure S8a–c, S8d–F)

and coalesced tetramers (Figure S9), tiny holes can be observed on the order of 1 nm down to several Au atoms in diameter. As expected, these voids are a result of joining three or more two-dimensional spherical surfaces within a three-dimensional Euclidean space. Following thermal treatment, the shrinking of these voids can be followed until a solid polygonal structure is achieved (Figure S8a–c, S10), concurrent with the fusion of the Au atomic stages (Figure S8d–f). In one case we could observe the coalescence of three AuNPs from a tetrameric assembly (Figure S11a–f) following thermal treatment. In each case, the coalescence of prearranged AuNPs is an example of a template-directed process that would not be present in the absence of the molecular templating interactions, as proximity and precise spatial arrangements are key components for the coalescence of AuNPs into more permanent predetermined polygonal structures.

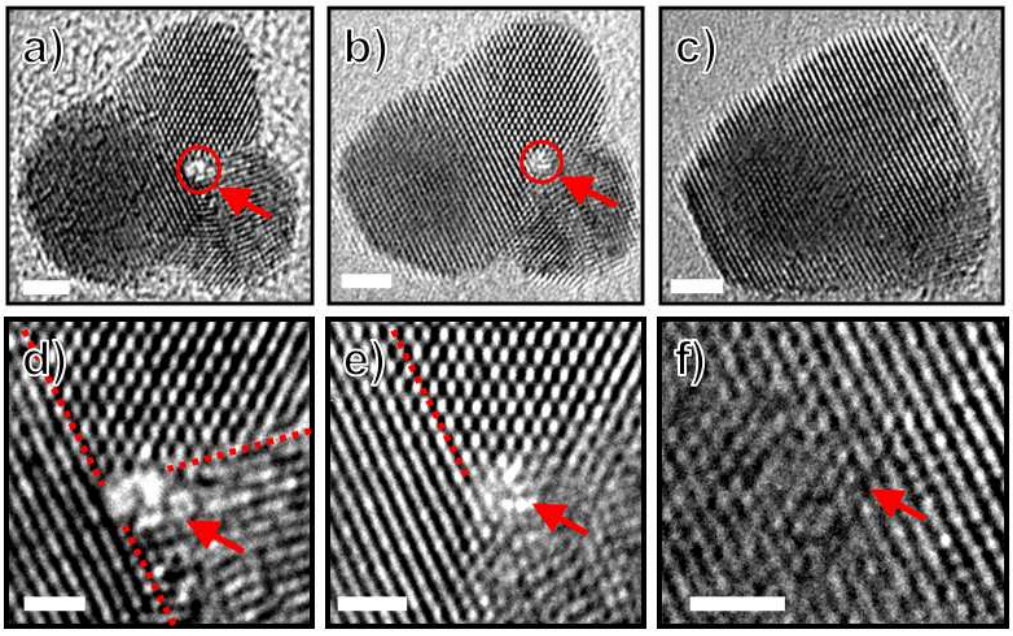

Figure S8. HR-TEM images following the coalescence of a trimeric nanoparticle arrangement (a–c, d–f). The fusion of three different atomic lattices (d) can be observed (d–f) concurrent with the diminishing of the central void over time. Scale bars = 2 nm (a–c), 1 nm (d–f)

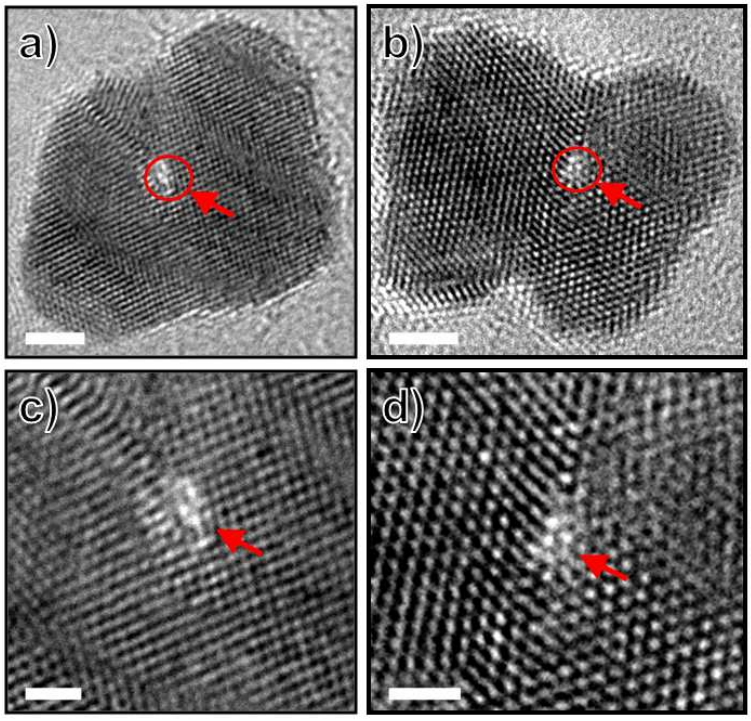

Figure S9. HR-TEM images of two coalesced tetrameric nanoparticle assemblies (a, b) each having a central void (c, d) several atoms in diameter. Scale bars = 2 nm (a, b), 1 nm (c, d)

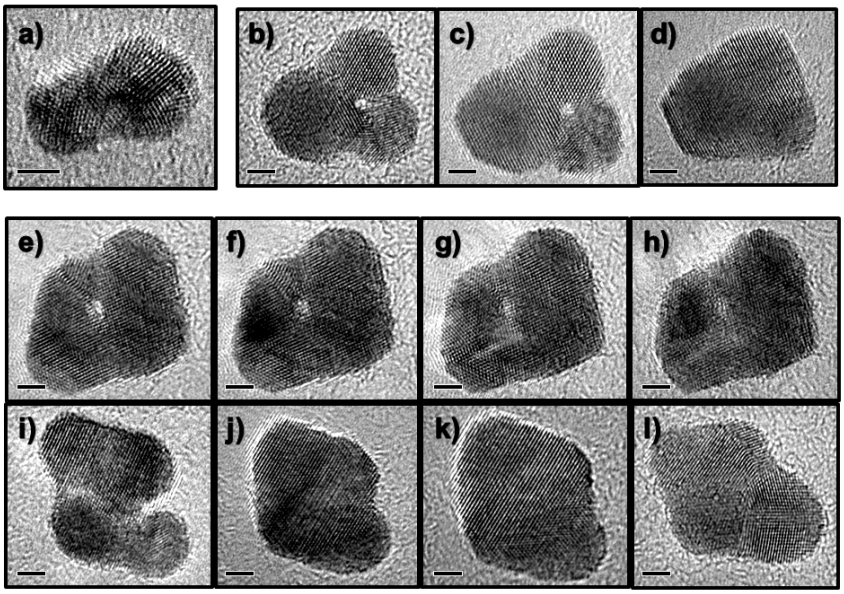

Figure S10. Representative high-resolution transmission electron microscopy (TEM) images following the template-directed coalescence of the homo-dimers (a), trimers (b–d), and tetramers (e–h; i–k) into rod-like, triangular, and square-like nanostructures, following electron ablation, and an additional example (l) of a template-directed coalesced square-like nanostructure. Scale bars = 2 nm.

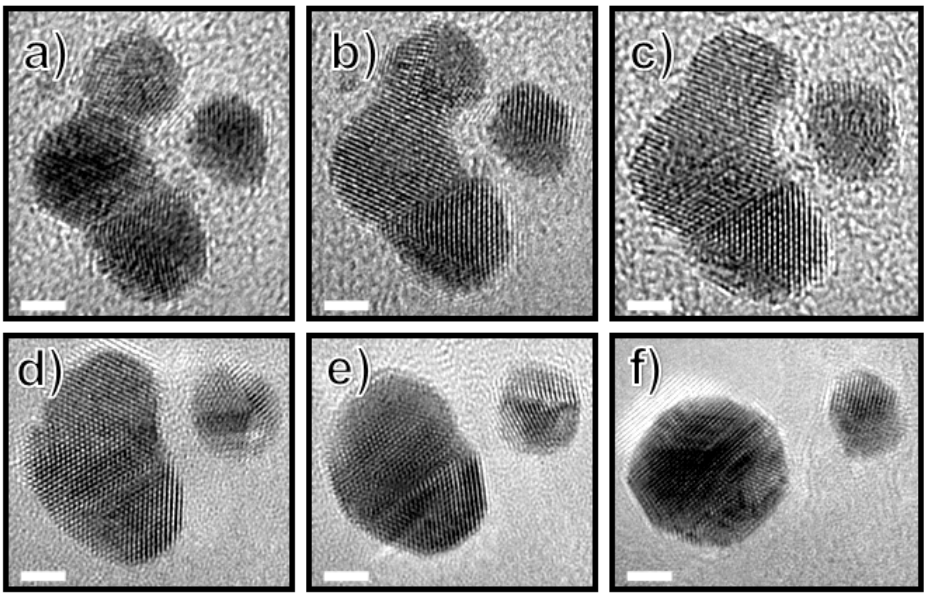

Figure S11. HR-TEM images following the coalescence (a–f) of three AuNPs from a molecular templated tetrameric assembly. Scale bars = 2 nm (a–f).

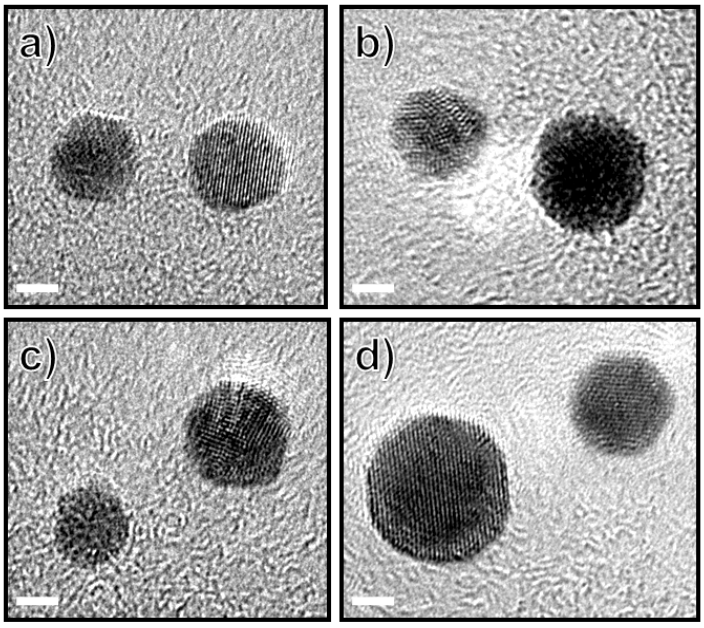

Figure S12. Typical HR-TEM images of molecular templated AuNP dimers. Scale bars = 2 nm (a–d)

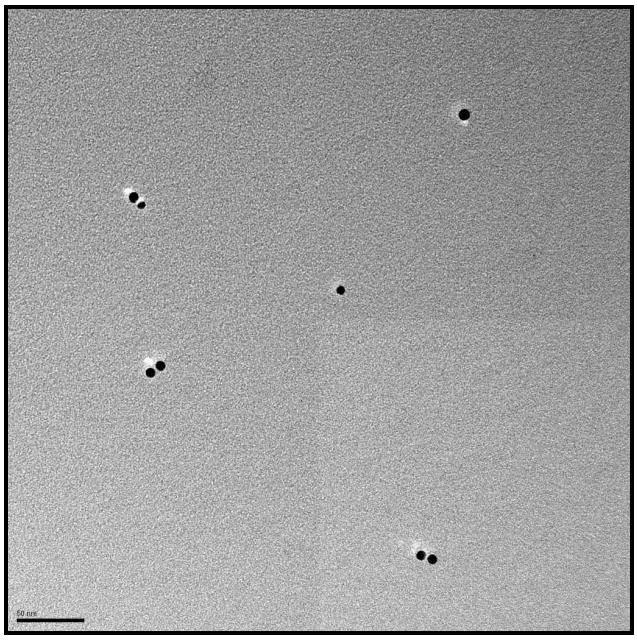

Figure S13. Typical LR-TEM image of molecular templated AuNP dimers. Scale bars = 50 nm

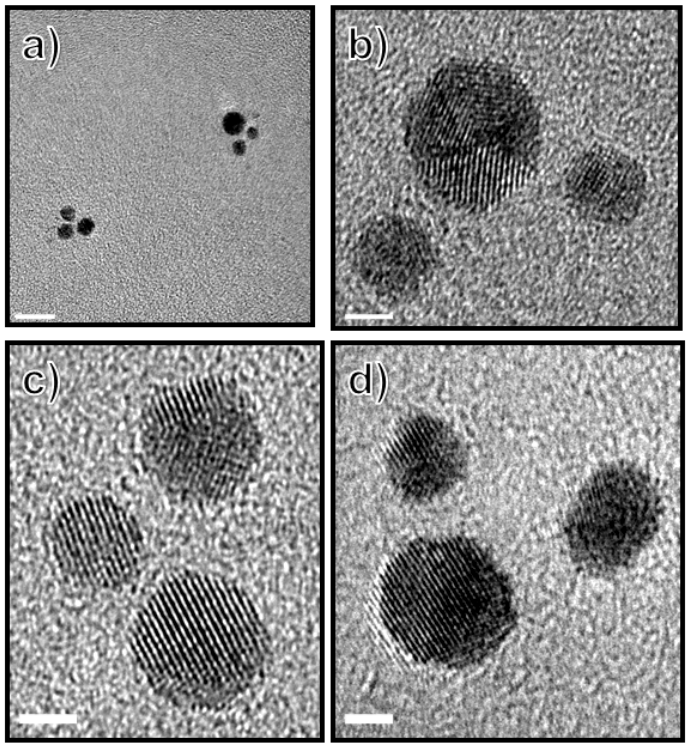

Figure S14. Typical HR-TEM images of molecular templated AuNP trimers. Scale bars = 10 nm (a), 2 nm (b–d)

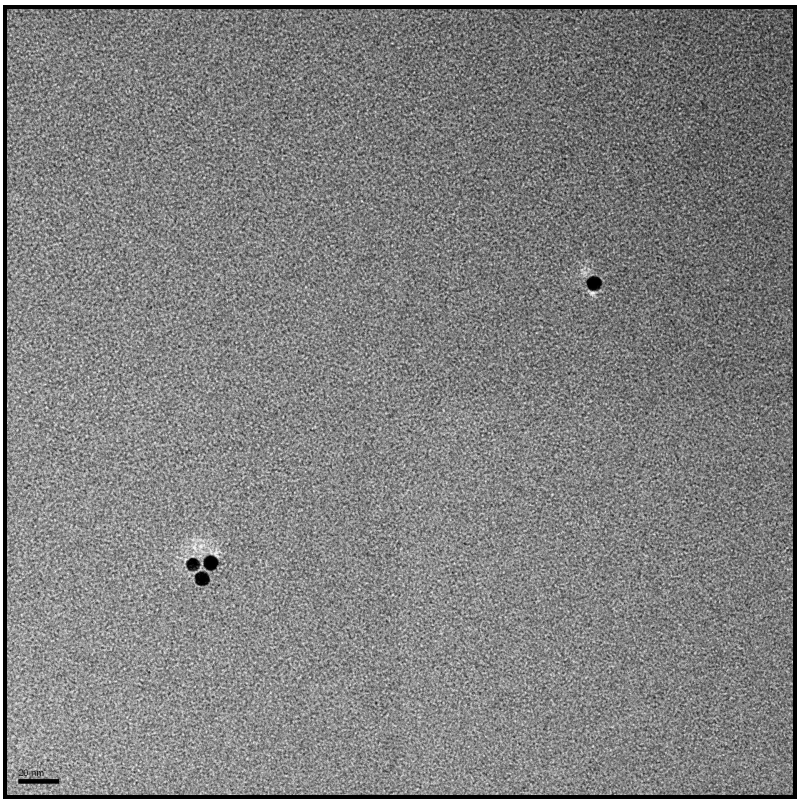

Figure S15. Typical LR-TEM image of molecular templated AuNP trimers. Scale bars = 20 nm.

Isothermal Titration Microcalorimetry

To study the thermodynamics of psuedorotaxane formation, isothermal titration microcalorimetry (ITC) measurements were performed in order to construct the binding isotherm (Figure S16) and determine the thermodynamic parameters (ΔH^o, ΔS^o, ΔG^o) and ultimately the association constant (K_a) values characterizing the binding of TTF-DEG with the alkyne-functionalized $CBPQT^{4+}$ derivatives. For the complexation of TTF-DEG with the alkyne-functionalized $CBPQT^{4+}$ derivative, the value of K_a was determined to be 1.15×10^5 M^{-1}, giving rise to a ΔH^o value of -11.4 ± 0.1 kcal·mol^{-1} and a ΔS^o value of -15.1 ± 0.2 cal·mol^{-1}·K^{-1}, corresponding to a ΔG^o of -6.92 ± 0.05 kcal·mol^{-1} at 298 K in MeCN.

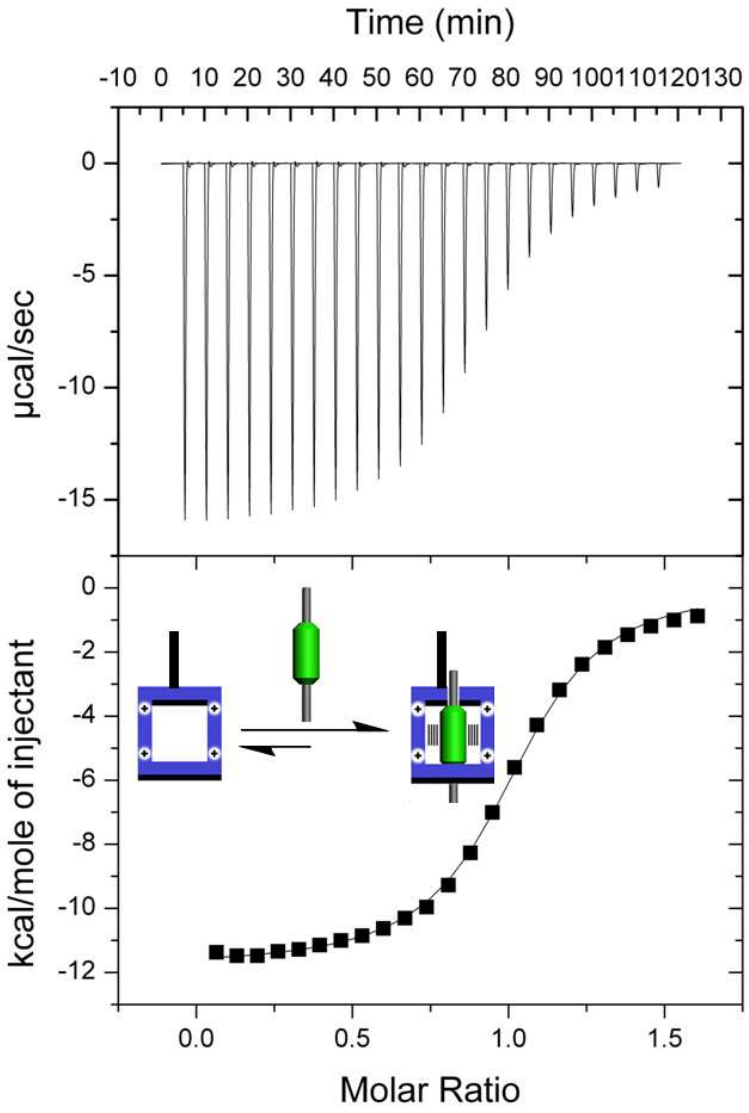

Figure S16. Isothermal titration microcalorimetry binding isotherm for the complexation of TTF-DEG with the host $CBPQT^{4+}$ ring.

Crystallographic Data-based Semiempirical Distance Estimation

By reference to crystallographic data previously obtained[S11] for $CBPQT^{4+}$ complexes with TTF (Figure S17) and diethyleneglycol-disubstituted 1,5-dihydroxynaphthalene guests (DNP-DEG) (Figure S18), along with the solid-state crystal structure of thioctic acid (Figure S18),[S12] it has been estimated that each $CBPQT^{4+}$ ring is positioned approximately 0.792 nm from the AuNP

surface when bound to a TTF dithiolane ligand. Figure S18 illustrates the distance from one end oxygen atom to the opposite end oxygen atom of the diethyleneglycol-disubstituted 1,5-dihydroxynaphthalene while complexed with $CBPQT^{4+}$. The solid state crystal structure of thioctic acid (Figure S18), starting from one of the sulfur atoms to the oxygen atom of the carboxylic acid moiety has a measured distance of 0.792 nm. Therefore, it is estimated that the $CBPQT^{4+}$ ring, when complexed with a TTF-DEG recognition units bearing a thioctic acid moiety, sits approximately 0.792 nm from the AuNP when thioctic acid sulfur atoms are bound to the Au surface. Overall these dimensions correlate well with the distances observed by TEM for the template-directed AuNP assemblies, where the molecular template may sit in numerous positions and still remain in contact and bound with the AuNPs.

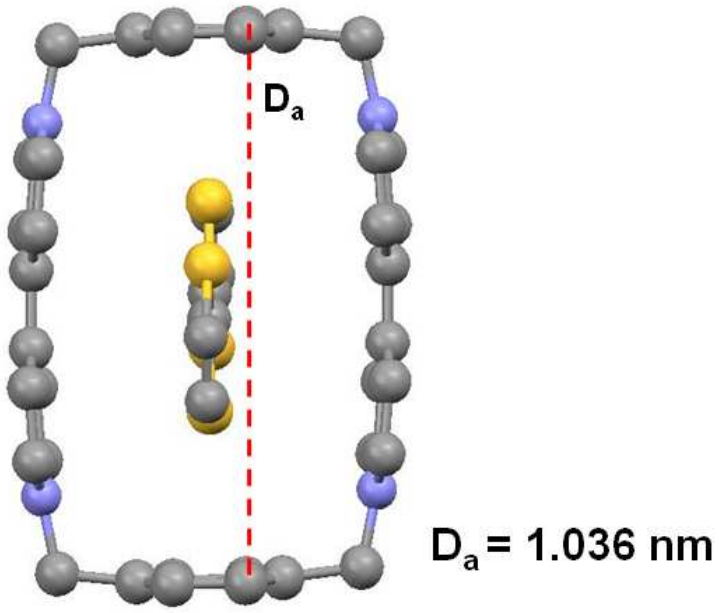

Figure S17. A ball-and-stick representation of the solid-state structure of a psuedorotaxane formed by the complexation of TTF by the $CBPQT^{4+}$ ring illustrating the length of the host ring ($\mathbf{D}_a$)

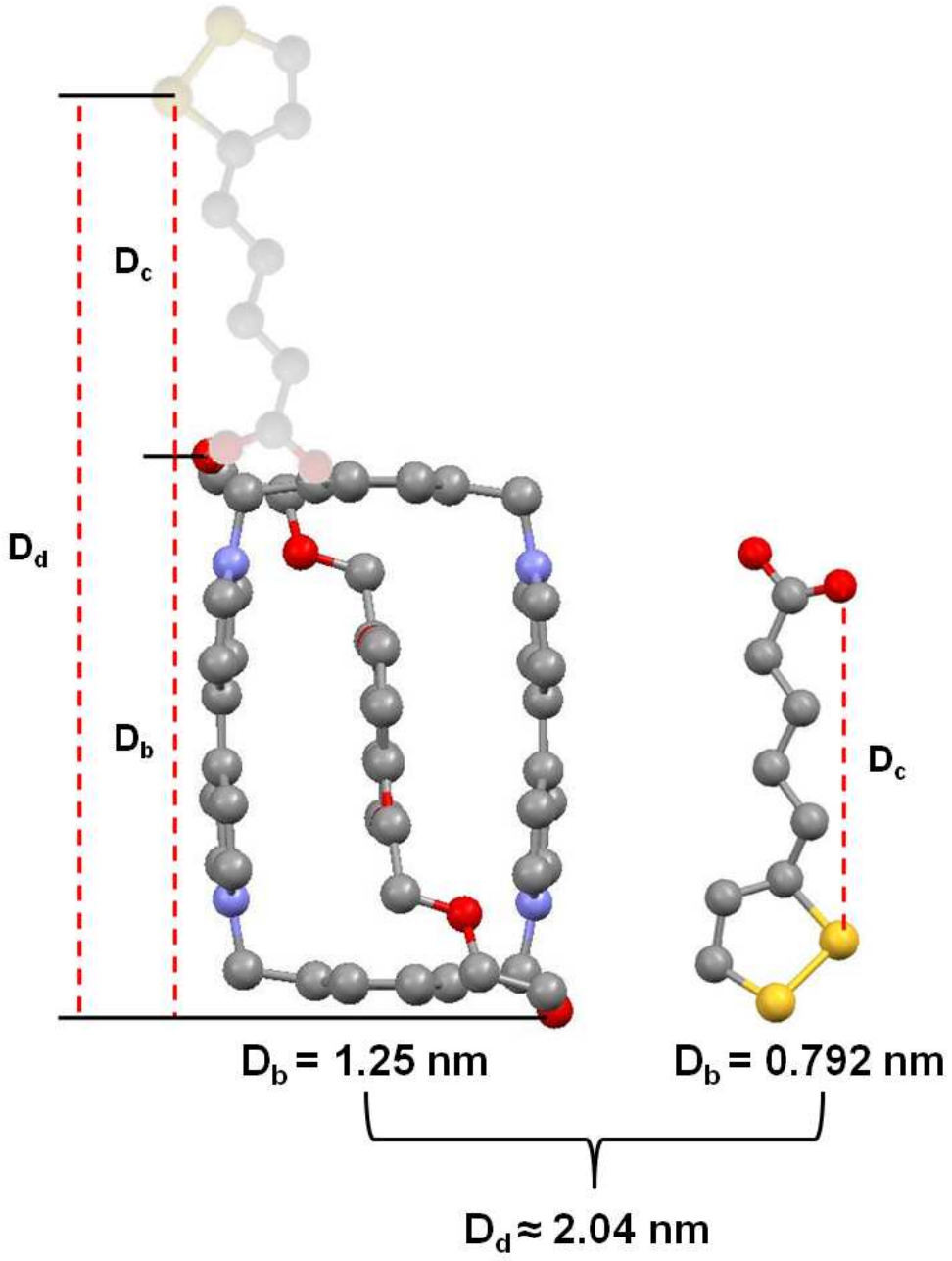

Figure S18. A ball-and-stick representation of the solid-state structure of a pseudorotaxane formed by the complexation of diethyleneglycol-disubstituted 1,5-dihydroxynaphthalene by the $CBPQT^{4+}$ ring (left) and thioctic acid (right) illustrating the length of the host ring ($\mathbf{D}_b$) and the length of thioctic acid from a single sulfur atom ($\mathbf{D}_c$). Length $\mathbf{D}_d$ illustrates the estimated total length of a psuedorotaxane formed between a thioctic acid functionalized diethyleneglycol-disubstituted 1,5-dihydroxynaphthalene and the $CBPQT^{4+}$ ring where 0.792 nm is the estimated distance from the host ring to the sulfur atom of the thioctic acid moiety.

References

S1. Klajn, R.; Fang, L.; Coskun, A.; Olson, M. A.; Wesson, P. J.; Stoddart, J. F.; Grzybowski, B. A. *J. Am. Chem. Soc.* **2009**, *131*, 4233–4235.

S2. Braunschweig, A. B.; Dichtel, W. R.; Miljanić, O. Š.; Olson, M. A.; Spruell, J. M.; Khan, S. I.; Heath, J. R.; Stoddart, J. F. *Chem. Asian J.* **2007**, *2*, 634–647.

S3. Haridas, V.; Lai, K.; Sharma, Y. K.; Upreti, S. *Org. Lett.* **2008**, *10*, 1645–1647.

S4. Heyer, D.; Lehn, J.-M. *Tetrahedron Lett.* **1986**, *27*, 5869–5872.

S5. Sunberg, R. J.; Suter, S. R.; Brenner, M.; *J. Am. Chem. Soc.* **1972**, *94*, 513–520.

S6. Anelli, P.-L.; Ashton, P. R.; Ballardini, R.; Balzani, V.; Delgado, M.; Gandolfi, M. T.; Goodnow, T. T.; Kaifer, A. E.; Philp, D.; Pietraszkiewicz, M.; Prodi, L.; Reddington, M. V.; Slawin, A. M. Z.; Spencer, N.; Stoddart, J. F.; Vicent, C.; Williams, D. J. *J. Am. Chem. Soc.* **1992**, *114*, 193–218

S7. Liu, Y.; Ke, C.-F.; Zhang, H.-Yi.; Cui, J.; Ding, F. *J. Am. Chem. Soc.* **2008**, *130*, 600–605.

S8. (a) Manna, A.; Chen, P. L.; Akiyama, H.; Wei, T. X.; Tamada, K.; Knoll, W., *Chem. Mater.* **2003**, *15*, 20–28. (b) Leff, D. V.; Ohara, P. C.; Heath, J. R.; Gelbart, W. M. *J. Phys. Chem.* **1995**, *99,* 7036-7041.

S9. (a) Jorgensen, W. L.; Tirado-Rives, J. *J. Am. Chem. Soc.* **1988**, *110*, 1657−1666. (b) Tirado-Rives, J; Jorgensen, W. L. *J. Am. Chem. Soc.* **1990**, *112*, 2773−2781. (c) Jorgensen, W. L.; Nguyen, T. B. *J. Comp. Chem.* **1993**, *13*, 195−205. (d) Jorgensen, W. L.; Maxwell, D. S.; Tirado-Rives, J. *J. Am. Chem. Soc.* **1996**, *118*, 11225−11236. (e) Jorgensen, W. L. *OPLS Force Fields, Encyclopedia of Computational Chemistry*, Schleyer (Ed.), Wiley: New York, **1998**, vol. 3, 1986–1989.

S10. (a) Klajn, R., Bishop, K. J. M., Fialkowski, M., Paszewski, M., Campbell, C. J., Gray, T. P., Grzybowski, B. A. *Science* **2007**, *316*, 261-264. (b) Klajn, R., Gray, T. P., Wesson, P. J., Myers, B. D., Dravid, V. P., Smoukov, S. K., Grzybowski, B. A. *Adv. Funct. Mater.* **2008**, *18*, 2763-2769.

S11. Olson, M. A.; Braunschweig, A. B.; Fang, L.; Ikeda, T.; Klajn, R.; Trabolsi, A.; Wesson, P. J.; Benítez, D.; Mirkin, C. A.; Grzybowski, B. A.; Stoddart, J. F. *Angew. Chem. Int. Ed*. **2009,** *10*, 1792–1797.

S12. Reed, L. J.; DeBusk, B. G.; Gunsalus, I. C.; Hornberger, C. S. *Science* **1951**, *114,* 93–94.